Supplemental Material: Characterization of the airborne aerosol inlet and transport system used during the A-LIFE aircraft field experiment

Manuel Schöberl[1,2], Maximilian Dollner[1], Josef Gasteiger[1,a], Petra Seibert[3,4], Anne Tipka[1,3,b], and Bernadett Weinzierl[1]

[1]University of Vienna, Faculty of Physics, Aerosol Physics and Environmental Physics, 1090 Vienna, Austria
[2]University of Vienna, Vienna Doctoral School in Physics, 1090 Vienna, Austria
[3]University of Vienna, Department of Meteorology and Geophysics, 1090 Vienna, Austria
[4]University of Natural Resources and Life Sciences, Institute of Meteorology and Climatology, 1180 Vienna, Austria
[a]now at: Hamtec Consulting GmbH @ EUMETSAT, Darmstadt, Germany
[b]now at: International Data Centre, Comprehensive Nuclear-Test-Ban Treaty Organization, PO Box 1200, 1400 Vienna, Austria

Correspondence to: Bernadett Weinzierl (bernadett.weinzierl@univie.ac.at)

S1 A-LIFE In-Cabin Instrumentation

Table S1 lists aerosol instruments that were installed in the aircraft cabin of the Falcon and were connected to the isokinetic inlet during the A-LIFE mission. The instrument setup including the flows in the different sampling line parts can be seen in Figure S1. Two experimental instruments which drew together 2.85 l min^{-1} are not included in Table S1 and Figure S1.

In total, the A-LIFE instrumentation drew a volumetric flow of a minimum of 17.87 l min^{-1} which could increase to a maximum of 22.83 l min^{-1}. The value of the total flow varies because two impactor devices were only turned on during selected measurement periods (typically six times for 5-10 minutes per flight) which increased the total flow by 0.96 l min^{-1} (Kandler et al., 2007) during these periods. Furthermore, the so-called constant pressure inlet (CPI) system of the DMT Cloud Condensation Nuclei Counter (CCNC) caused a varying flow depending on altitude. The inlet system of the CCNC was used to ensure measurements at a fixed pressure of 500 hPa. The CPI system consists of two orifices with different diameters used at different altitudes, and a pump. Depending on the ambient pressure, the pump regulated the flow (between 0 and 4 l min^{-1}) so that a pressure of 500 hPa was established behind the orifice.

S2 Aerosol Number Size Distribution

For the derivation of the aerosol number size distribution (NSD) for each of the 262 A-LIFE flight sequences, the data of four instruments were used. The instruments and the size ranges, used for the combined NSDs, are summarized in Table S2.

As explained in Section 2.3 in the main manuscript, the refractive index needed for the derivation of the NSD from OPC measurements is inferred from the aerosol composition along the flight track based on a mixture of five main aerosol types determined with the FLEXPART model (Stohl et al., 1998, Seibert and Frank, 2004). The corresponding refractive indices for each of the five aerosol types are based on literature and are summarized in Table S3. Since the size distribution of CAS is measured at ambient relative humidity conditions, but the other instruments contributing to the combined NSD measure at dry conditions, a growth factor is needed to convert the

CAS NSDs to dry particle diameters. The growth factors are dependent on the particle composition, and were also derived based on FLEXPART-modelled aerosol particle composition. The corresponding hygroscopicity of the five aerosol types are also included in Table S3.

Table S1: Overview of the in-cabin instrumentation which was connected to the isokinetic inlet during A-LIFE.

Instrument	Manufacturer	Nominal flow [lpm]	Tubing length [m]	Measured quantity
CPC1	TSI	1	5.83	Integral particle number concentration
CPC2	TSI	1.5	2.66	Integral particle number concentration
CPSA1	Custom-built at DLR	1	2.39	Integral non-volatile particle number concentration
CPSA2	Custom-built at DLR	1	2.47	Integral non-volatile particle number concentration
CPSA3	Custom-built at DLR	1	2.22	Integral particle number concentration
SkyOPC	Grimm	1.2	1.52	Aerosol number size distribution
SkyOPCTD	Grimm	1.2	3.49	Non-volatile aerosol number size distribution
Impactor device 1	Custom-built at TU Darmstadt	0.48	0.92	Chemical particle composition, shape
Impactor device 2	Custom-built at TU Darmstadt	0.48	1.02	Chemical particle composition, shape
SP2 (+ Bypass)	DMT	0.12 (+ 2)	1.59	Refractory black carbon mass
CCNC (+ CPI)	DMT	1 (+ 0-4)	2.85	Number concentration of cloud condensation nuclei at various supersaturations
Aurora 4000 Nephelometer	Ecotech	2	2.68	Scattering coefficient at three wavelengths (450, 525 and 635 nm)
TAP	Brechtel	2	3.52	Absorption coefficient at three wavelengths (467, 528 and 652 nm)

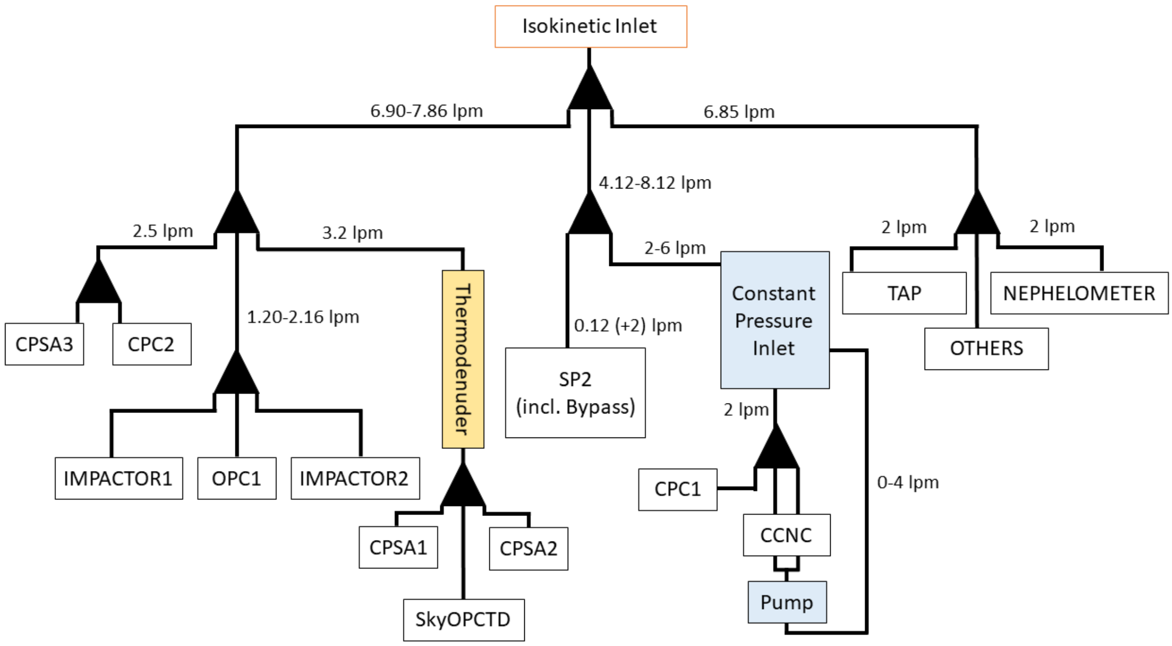

Figure S1: Flow plan of the in-cabin instrumentation that was connected to the isokinetic inlet. Note, this flow plan shows the default setup for the A-LIFE campaign which was flown almost the entire time. However, for testing purposes, it was also possible to operate the SkyOPCTD without thermodenuder or behind the constant pressure inlet.

Table S2: Instrumentation used for the derivation of the aerosol number size distribution (NSD) for each of the 262 A-LIFE flight sequences.

Instrument Type	Instrument Model	Size Range Used for Combined NSD	Location	Time Resolution
Condensation Particle Counter	TSI3760a (CPC2)	D_p > 10 nm	In-cabin (particles measured at dry conditions)	1 Hz
Optical Particle Counter	Grimm SkyOPC 1.129 (SkyOPC)	280 nm < D_p < 3 µm (for in-cabin NSD) 280 nm < D_p < 1 µm (for out-cabin NSD)	In-cabin (particles measured at dry conditions)	1 Hz
Optical Particle Counter	DMT Ultra High Sensitivity Aerosol Spectrometer – Airborne (UHSAS-A)	125 nm < D_p < 400 nm	Mounted under the aircraft wing (actively-pumped and dried sample flow)	1 Hz
Optical Particle Counter	DMT Cloud and Aerosol Spectrometer (UNIVIE CAS)	0.9 µm < D_p < 50 µm (for out-cabin NSD only)	Mounted under the aircraft wing (passive flow; particles measured at ambient relative humidity conditions)	1 Hz

Table S3: Refractive index (at dry relative humidity) and hygroscopicity parameters used for the derivation of the aerosol NSD including corresponding references. Table modified from Dollner (2022).

Aerosol Type	Refractive Index	Reference	Hygroscopicity Parameter κ	Reference
Black Carbon	n = 1.75-1.95 k = 0.63-0.79	Bond and Bergstrom, 2006	$\kappa = 0$	-
Sulfate	n = 1.50-1.53 k = 0	Flores et al., 2012; Tang, 1996; Toon et al., 2006	$\kappa = 0.483$	Good et al., 2010
Organic Matter	n = 1.44-1.61 k = 0-0.03	Moise et al., 2015	$\kappa = 0.163$	Petters and Kreideweis, 2007
Dust	size dependent (see Kandler et al., 2011)	Kandler et al., 2011	$\kappa = 0.03$	Herich et al., 2009
Sea salt	n = 1.541 k = 0	Eldrige and Palik, 1985	$\kappa = 1.1$	Zieger et al., 2017

S3 Transport Efficiency

In this study, the transport efficiency was calculated with empirical equations from literature. For Figure 6 in the main manuscript, the inlet efficiency was derived with the experimentally determined sampling efficiency (inlet + transport efficiency) and the calculated transport efficiency. For this, the transport efficiency of the SkyOPC was used. The transport system for the SkyOPC is summarized in Table S4. The volumetric flow, the length as well as the bend angles were used for the calculation of the efficiency of each tubing part. For the first four sampling line pieces the mean of the flow range was used. The inner diameter of all 9 tubing parts is 4.572 mm.

For the losses of coarse mode aerosol particles in the tubing system, two loss mechanisms were considered: losses in tubing bends and sedimentation losses. For all calculations, the aerosol particle itself was assumed to be a mineral dust particle (density $\rho = 2.6\ \mathrm{g\ cm^{-3}}$ and shape factor $\chi = 1.2$; Hess et al., 1998 and Kaaden et al., 2008).

S3.1 Particle Losses in Bends

For aerosol particle losses in bends of sampling lines, the following equation given by Pui et al., 1987 was used:

$$\eta_{\mathrm{bend}} = \left(1 + \left(\frac{\mathrm{Stk}}{0.171}\right)^{0.452\frac{\mathrm{Stk}}{0.171}+2.242}\right)^{-\frac{2}{\pi}\theta} \qquad \text{(S1)}$$

Here, θ is the angle of curvature of the sampling line in degrees and Stk represents the Stokes number. For the calculation of the Stokes number, the following equations were used (S2-S5; Seinfeld and Pandis, 2016):

$$\eta = 1.7188 \cdot 10^{-5} \left[\left(\frac{\mathrm{T}}{273.15}\right)^{1.5}\left(\frac{384.15}{\mathrm{T}+111}\right)\right] \qquad \text{(S2)}$$

$$\lambda = 0.0651 \frac{\eta}{1.8 \cdot 10^{-5}} \frac{1013}{p} \sqrt{\frac{T}{298}} \tag{S3}$$

$$C_C = 1 + \frac{2\lambda}{D_p} \left[1.257 + 0.4 \exp\left(\frac{-1.1\, D_p}{2\lambda}\right)\right] \tag{S4}$$

$$Stk = \frac{\rho\, {D_p}^2\, C_c \left(\frac{v_{TAS}}{7.1}\right)}{18\, \eta\, D\, \chi} \tag{S5}$$

Here, η is the dynamic viscosity of air, λ the mean free path of the ambient air, Cc the Cunningham slip correction factor. p represents the ambient pressure, while T is the temperature inside the aircraft cabin respectively inside the sampling line, which is assumed to be 30°C. D represents the inner diameter of the sampling line.

S3.2 Sedimentation Losses

For aerosol particle losses in bends of sampling lines, the following equation given by Thomas (1958) and Fuchs (1964) was used:

$$\eta_{sed} = 1 - \frac{2}{\pi}\left(2\, \epsilon \sqrt{1 - \varepsilon^{\frac{2}{3}}} - \varepsilon^{\frac{1}{3}} \sqrt{1 - \varepsilon^{\frac{2}{3}}} + \arcsin \sqrt[3]{\epsilon}\right) \tag{S6}$$

$$\text{with } \epsilon = \frac{3\, L\, v_{TS}}{4\, D\, Q} \cdot \cos\theta \tag{S7}$$

given by Heyder and Gebhart (1977). Here, θ is the angle of inclination, L the length of the sampling line, Q the volumetric flow, D the inner diameter of the sampling line and v_{TS} the particle terminal settling velocity, which was calculated with the following equation (Seinfeld and Pandis, 2016):

$$v_{TS} = \frac{\rho\, {D_p}^2\, C_c\, g}{18\, \eta\, \chi} \tag{S8}$$

Table S4: Overview of all sampling line pieces which formed the transport system of the SkyOPC.

Sampling line	Flow [lpm]	Length [m]	Bend angle [°]
#1	6.90-7.86	0.14	80
#2	6.90-7.86	0.12	0
#3	1.20-2.16	0.12	0
#4	1.20-2.16	0.12	0
#5	1.2	0.25	90
#6	1.2	0.30	0
#7	1.2	0.25	90
#8	1.2	0.10	0
#9	1.2	0.12	0

S4 Fitted Ambient Pressure and Temperature

As explained in Section 2.4.3 in the main manuscript, we used the Stokes number Stk_{50} of each v_{TAS} value to convert back to a new cut-off diameter $D_{p,50}$. For this, we used fitted values of ambient pressure and temperature for the whole v_{TAS} range from 70 to 220 m s^{-1}. The used sigmoid fits for this approach are displayed in Figure S2 and Figure S3.

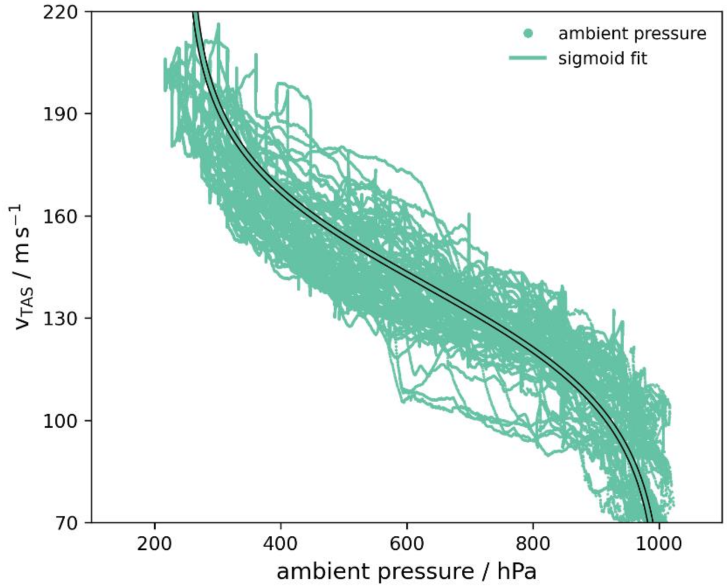

Figure S2: Ambient pressure as a function of v_{TAS}. The points show the 1 s data measured by the CMET system of the Falcon during the A-LIFE campaign. The straight line depicts the sigmoid fit which was used for the calculation of the cut-off diameters.

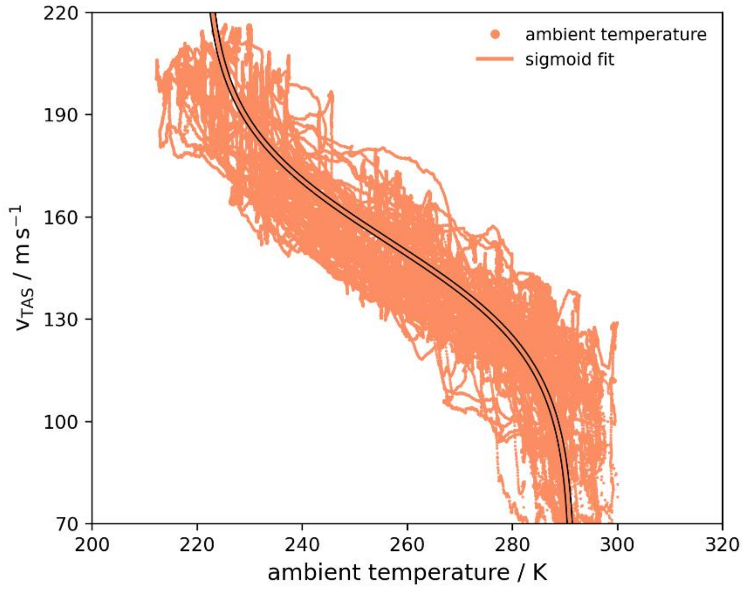

Figure S3: Ambient temperature as a function of v_{TAS}. The points show the 1 s data measured by the CMET system of the Falcon during the A-LIFE campaign. The straight line depicts the sigmoid fit which was used for the calculation of the cut-off diameters.

References

Bond, T. C. and Bergstrom, R. W.: Light Absorption by Carbonaceous Particles: An Investigative Review, Aerosol Sci. Technol., 40, 27–67, https://doi.org/10.1080/02786820500421521, 2006.

Dollner, M.: Assessment of the global distribution of coarse-mode aerosol and clouds with large-scale in situ aircraft observations, PhD thesis, Universität Wien, Vienna, https://doi.org/10.25365/THESIS.72087, 2022.

Eldridge, J. and Palik, E.: Handbook of Optical Constants of Solids, chap. Sodium Chloride, Academic Press, Inc., Orlando, FL, 775– 793, 1985.

Fuchs, N.: The Mechanics of Aerosols, Pergamon, Oxford, 1964.

Good, N., Topping, D. O., Allan, J. D., Flynn, M., Fuentes, E., Irwin, M., Williams, P. I., Coe, H., and McFiggans, G.: Consistency between parameterisations of aerosol hygroscopicity and CCN activity during the RHaMBLe discovery cruise, Atmospheric Chem. Phys., 10, 3189–3203, https://doi.org/10.5194/acp-10-3189-2010, 2010.

Herich, H., Tritscher, T., Wiacek, A., Gysel, M., Weingartner, E., Lohmann, U., Baltensperger, U., and Cziczo, D. J.: Water uptake of clay and desert dust aerosol particles at sub- and supersaturated water vapor conditions, Phys. Chem. Chem. Phys., 11, 7804, https://doi.org/10.1039/b901585j, 2009.

Hess, M., Koepke, P., & Schult, I.: Optical Properties of Aerosols and Clouds: The Software Package OPAC, B. Am. Meteor. Soc., 79, 831–844, doi:10.1175/15200477(1998)079<0831:OPOAAC>2.0.CO;2, 1998.

Heyder, J. and Gebhart, J.: Gravitational deposition of particles from laminar aerosol flow through inclined circular tubes, J. Aerosol Sci., 8, 289–295, https://doi.org/10.1016/0021-8502(77)90048-9, 1977.

Kaaden, N., Massling, A., Schladitz, A., Müller, T., Kandler, K., Schütz, L., Weinzierl, B., Petzold, A., Tesche, M., Leinert, S., Deutscher, C., Ebert, M., Weinbruch, S., and Wiedensohler, A.: State of mixing, shape factor, number size distribution, and hygroscopic growth of the Saharan anthropogenic and mineral dust aerosol at Tinfou, Morocco, Tellus B Chem. Phys. Meteorol., 61, 51–63, https://doi.org/10.1111/j.1600-0889.2008.00388.x, 2009.

Kandler, K., Benker, N., Bundke, U., Cuevas, E., Ebert, M., Knippertz, P., Rodríguez, S., Schütz, L., and Weinbruch, S.: Chemical composition and complex refractive index of Saharan Mineral Dust at Izaña, Tenerife (Spain) derived by electron microscopy, Atmos. Environ., 41, 8058–8074, https://doi.org/10.1016/j.atmosenv.2007.06.047, 2007.

Kandler, K., Lieke, K., Benker, N., Emmel, C., Küpper, M., Müller-Ebert, D., Ebert, M., Scheuvens, D., Schladitz, A., Schütz, L., and Weinbruch, S.: Electron microscopy of particles collected at Praia, Cape Verde, during the Saharan Mineral Dust Experiment: particle chemistry, shape, mixing state and complex refractive index, Tellus B Chem. Phys. Meteorol., 63, 475–496, https://doi.org/10.1111/j.1600-0889.2011.00550.x, 2011.

Michel Flores, J., Bar-Or, R. Z., Bluvshtein, N., Abo-Riziq, A., Kostinski, A., Borrmann, S., Koren, I., Koren, I., and Rudich, Y.: Absorbing aerosols at high relative humidity: linking hygroscopic growth to optical properties, Atmospheric Chem. Phys., 12, 5511–5521, https://doi.org/10.5194/acp-12-5511-2012, 2012.

Moise, T., Flores, J. M., and Rudich, Y.: Optical Properties of Secondary Organic Aerosols and Their Changes by Chemical Processes, Chem. Rev., 115, 4400–4439, https://doi.org/10.1021/cr5005259, 2015.

Petters, M. D. and Kreidenweis, S. M.: A single parameter representation of hygroscopic growth and cloud condensation nucleus activity, Atmospheric Chem. Phys., 7, 1961–1971, https://doi.org/10.5194/acp-7-1961-2007, 2007.

Pui, D. Y. H., Romay-Novas, F., and Liu, B. Y. H.: Experimental Study of Particle Deposition in Bends of Circular Cross Section, Aerosol Sci. Technol., 7, 301–315, https://doi.org/10.1080/02786828708959166, 1987.

Seibert, P. and Frank, A.: Source-receptor matrix calculation with a Lagrangian particle dispersion model in backward mode, Atmospheric Chem. Phys., 4, 51–63, https://doi.org/10.5194/acp-4-51-2004, 2004.

Seinfeld, J. H. and Pandis, S. N.: Atmospheric chemistry and physics: from air pollution to climate change, Third edition., John Wiley & Sons, Hoboken, New Jersey, 1 pp., 2016.

Stohl, A., Hittenberger, M., and Wotawa, G.: Validation of the lagrangian particle dispersion model FLEXPART against large-scale tracer experiment data, Atmos. Environ., 32, 4245–4264, https://doi.org/10.1016/S1352-2310(98)00184-8, 1998.

Tang, I. N.: Chemical and size effects of hygroscopic aerosols on light scattering coefficients, J. Geophys. Res. Atmospheres, 101, 19245–19250, https://doi.org/10.1029/96JD03003, 1996.

Thomas, J. W.: Gravity Settling of Particles in a Horizontal Tube, J. Air Pollut. Control Assoc., 8, 32–34, https://doi.org/10.1080/00966665.1958.10467825, 1958.

Toon, O. B., Pollack, J. B., and Khare, B. N.: The optical constants of several atmospheric aerosol species: Ammonium sulfate, aluminum oxide, and sodium chloride, J. Geophys. Res., 81, 5733–5748, https://doi.org/10.1029/JC081i033p05733, 1976.

Zieger, P., Väisänen, O., Corbin, J. C., Partridge, D. G., Bastelberger, S., Mousavi-Fard, M., Rosati, B., Gysel, M., Krieger, U. K., Leck, C., Nenes, A., Riipinen, I., Virtanen, A., and Salter, M. E.: Revising the hygroscopicity of inorganic sea salt particles, Nat. Commun., 8, 15883, https://doi.org/10.1038/ncomms15883, 2017.